LATTICE BOLTZMANN SIMULATION OF FLUID FLOW INDUCED BY THERMAL EFFECT IN HETEROGENEITY POROUS MEDIA

by

Peng HOU[a], Yang JU[a,b*], Chengzheng CAI[a], Lin GAO[a], and Shanjie SU[a]

[a] State Key Laboratory for Geomechanics and Deep Underground Engineering, China University of Mining and Technology, Xuzhou, China
[b] State Key Laboratory of Coal Resources and Safe Mining, China University of Mining and Technology, Beijing, China

Original scientific paper
https://doi.org/10.2298/TSCI17S1193H

In this paper, a coupled lattice Boltzmann model is used to visually study fluid flow induced by thermal effect in heterogeneity porous media reconstructed by the quartet structure generation set. The fluid flow behavior inside porous media is presented and analyzed under different conditions. The simulation results indicate that the pore morphological properties of porous media and the Rayleigh number have noticeable impact on the velocity distribution and flow rate of fluid.

Key words: *thermal effect, fluid flow, heterogeneity porous media, lattice Boltzmann model*

Introduction

Unconventional natural gas (including coal-bed gas and shale gas) and geothermal energy have become important clean energies with the remarkable advantages of abundant reserves, and their development and utilization will hopefully deal with the urgent demands for clean energy [1-3]. However, unconventional natural gas reservoir has extremely low permeability, hence effective stimulation of the reservoirs is usually used. The heat injection is an effective technique to increase the reservoirs permeability [4]. In the heat injection process, a thermal gradient will be generated along the heat injection direction. On the contrary, a thermal gradient will be also formed along the extraction direction in extraction of geothermal energy. Fluid migration will be ultimately induced by the thermal gradient [5], which is closely related to production efficiency. In deep reservoirs, as we known, fluid transport is invisible and complex due to heterogeneity and complex surroundings of reservoirs.

Lattice Boltzmann method (LBM), as a mesoscopic simulation method, is often employed to visually simulate fluid dynamics in complex porous media. The LBM brings many advantages over the conventional grid-based CFD methods, particularly in dealing with complex boundaries and parallelization of the algorithm [6]. In present, the LBM has been widely used to simulate fluid flow caused by pressure difference and velocity difference in complex porous media. The investigations of fluid flow induced by thermal effect are also often reported using the LBM, while these researches are generally carried out based on ideal and simple pore structure.

* Corresponding author, e-mail: juy@cumtb.edu.cn

To investigate fluid migration caused by thermal effect in heterogeneity porous media, a coupled LBM is established first. Then, the quartet structure generation set (QSGS) method is used to generate heterogeneity porous media. Finally, effects of pores structure, thermal gradient and Rayleigh number on fluid flow are simulated and analyzed using the established model.

Model description

Macroscopic description for fluid flow and heat transfer

In this study, incompressible fluid is assumed. Fluid migration caused by thermal effect involves fluid flow and heat transport, thus macroscopic governing equations for the fluid flow and heat transfer in the 2-D porous media are given [7]:

$$\partial_t \rho + \nabla(\rho \vec{\mathrm{u}}) = 0 \tag{1}$$

$$\partial_t(\rho \vec{\mathrm{u}}) + \nabla\left(\rho \vec{\mathrm{u}}\vec{\mathrm{u}}\right) = -\nabla p + \nabla^2(\rho \nu \vec{\mathrm{u}}) + \vec{\mathrm{F}} \tag{2}$$

$$\partial_t T + \nabla\left(\vec{\mathrm{u}}\, T\right) = \beta \nabla^2 T \tag{3}$$

where t is time, ρ – the density of fluid, $\vec{\mathrm{u}}$ – the velocity, p – the pressure, ν – the kinematic viscosity, T – the temperature, β – the thermal diffusivity, and $\vec{\mathrm{F}}$ – the body force.

Thermal effects are modelled by means of a Boussinesq approximation and the influence of the temperature is visible only through a body-force term. Therefore, the body force can be gained:

$$\vec{\mathrm{F}} = \mathrm{g}\alpha_T\left(T - T_0\right)\vec{\mathrm{j}} \tag{4}$$

where g is the gravitational acceleration, $\vec{\mathrm{j}}$ – the unit vector in the body force direction, T_0 – the reference temperature of fluid, and α_T – the thermal expansion coefficient of fluid.

The LBM description for fluid flow and heat transfer

Based on the idea of the lattice Boltzmann Bhatnagar-Gross-Krook (LBGK) model, the temperature can be treated as passive scalars [8]. Thus, fluid velocity and temperature can be treated individually. By following the popular BGK formulation, distribution functions can be described [9]:

$$f_i(\vec{\mathrm{x}} + c\vec{\mathrm{e}}_i\Delta t, t + \Delta t) - f_i(\vec{\mathrm{x}}, t) = -\frac{1}{\tau}\left[f_i(\vec{\mathrm{x}}, t) - f_i^{\mathrm{eq}}(\vec{\mathrm{x}}, t)\right] + \Delta t F_i \tag{5}$$

$$g_i(\vec{\mathrm{x}} + c\vec{\mathrm{e}}_i\Delta t, t + \Delta t) - g_i(\vec{\mathrm{x}}, t) = -\frac{1}{\tau}\left[g_i(\vec{\mathrm{x}}, t) - g_i^{\mathrm{eq}}(\vec{\mathrm{x}}, t)\right] \tag{6}$$

where $f_i(\vec{\mathrm{x}}, t)$ is the density distribution function at the lattice site $\vec{\mathrm{x}}$ and time t, $g_i(\vec{\mathrm{x}}, t)$ is the temperature distribution function at the lattice site $\vec{\mathrm{x}}$ and time t, $f_i^{\mathrm{eq}}(\vec{\mathrm{x}}, t)$ and $g_i^{\mathrm{eq}}(\vec{\mathrm{x}}, t)$ are the equilibrium distribution function, $c = \Delta x/\Delta t$ is the lattice speed with Δx and Δt as the lattice spacing and time step, respectively, and τ is the dimensionless relaxation time. For the D2Q9 (2-D nineteen-velocity) lattice model, the discrete lattice velocity $\vec{\mathrm{e}}_i$ are defined as $\vec{\mathrm{e}}_0 = (0,0)$, $\vec{\mathrm{e}}_1 = -\vec{\mathrm{e}}_3 = (1,0)$, $\vec{\mathrm{e}}_2 = -\vec{\mathrm{e}}_4 = (0,1)$, $\vec{\mathrm{e}}_5 = -\vec{\mathrm{e}}_7 = (1,1)$, and $\vec{\mathrm{e}}_6 = -\vec{\mathrm{e}}_8 = (-1,1)$.

The equilibrium distribution functions $f_i^{\mathrm{eq}}(\vec{\mathrm{x}}, t)$ and $g_i^{\mathrm{eq}}(\vec{\mathrm{x}}, t)$ and body force F_i for the D2Q9 lattice are given:

$$f_i^{\mathrm{eq}} = w_i \rho \left[1 + \frac{3\left(\vec{\mathrm{e}}_i \vec{\mathrm{u}}\right)}{c^2} + \frac{9\left(\vec{\mathrm{e}}_i \vec{\mathrm{u}}\right)^2}{2c^4} - \frac{3\left(\vec{\mathrm{u}}\vec{\mathrm{u}}\right)}{2c^2} \right] \tag{7}$$

$$g_i^{\mathrm{eq}} = w_i T \left[1 + \frac{3\left(\vec{\mathrm{e}}_i \vec{\mathrm{u}}\right)}{c^2} \right] \tag{8}$$

$$F_i = w_i \rho \left(1 - \frac{1}{2\tau} \right) \left[\frac{3\left(\vec{\mathrm{e}}_i \vec{\mathrm{F}}\right)}{c^2} + \frac{9\left(\vec{\mathrm{e}}_i \vec{\mathrm{u}}\right)\left(\vec{\mathrm{e}}_i \vec{\mathrm{F}}\right)}{c^4} - \frac{3\left(\vec{\mathrm{u}}\vec{\mathrm{F}}\right)}{c^2} \right] \tag{9}$$

where the weight factors ω_i are given by $\omega_0 = 4/9$, $\omega_{1-4} = 1/9$, and $\omega_{5-8} = 1/36$, respectively.

The macroscopic fluid variables, namely fluid density, ρ, velocity, $\vec{\mathrm{u}}$, and temperature, T, can be obtained from the distribution functions:

$$\rho = \sum_i f_i, \quad \rho \vec{\mathrm{u}} = \sum_i f_i \vec{\mathrm{e}}_i + \frac{\Delta t}{2} \rho \vec{\mathrm{F}} \quad T = \sum_i g_i \tag{10}$$

Additionally, to improve the stability and accuracy of numerical simulation, the regularization procedure is carried out in the study. The evolution equation for velocity field can be revised:

$$f_i(\vec{\mathrm{x}} + c\vec{\mathrm{e}}_i \Delta t, t + \Delta t) = f_i^{\mathrm{eq}}(\vec{\mathrm{x}}, t) + \left(1 - \frac{1}{\tau} \right) \tilde{f}_i^{\mathrm{noneq}} + \Delta t F_i \tag{11}$$

where $\tilde{f}_i^{\mathrm{noneq}}$ is the regularized distribution function, and for the D2Q9 model it can be given as:

$$\tilde{f}_i^{\mathrm{noneq}} = \omega_i \left[\frac{1}{2c_s^2} H^{(2)} \left(\frac{\vec{\mathrm{e}}_i}{c_s} \right) \sum_{\alpha=0}^{Q-1} f_\alpha^{\mathrm{noneq}} \vec{\mathrm{e}}_{\alpha j} \vec{\mathrm{e}}_{\alpha k} \right] \tag{12}$$

where $f_i^{\mathrm{noneq}} = f_i - f_i^{\mathrm{eq}}$ is the non-equilibrium part of the distribution function, and $H^{(2)}$ is the second order Hermite polynomial. For the temperature field, the same regularization procedure is implemented.

Model validation

The validation of the coupled LBM is carried out in two parallel porous plates with a thermal gradient and the natural convection flow. The upper plate and bottom plate are set as the cool and hot walls, respectively. The fluid with a constant normal flow is injected from the bottom plate and the same rate is discharged from the upper plate. At the same time, the upper plate with a constant velocity moves horizontally. The simulated size is Nx × Ny =100 × 50 lattices. The relaxation parameter, Reynolds number and Prandtl number are set as 1.0, 5 and 0.6, respectively. The periodic boundary is used in the horizontal direction. The velocity and temperature boundary conditions are both imposed on the top and bottom plates by the non-equilibrium extrapolation boundary.

The analytical solution of the velocity and temperature profile about the previous problem in steady-state can be expressed [10]:

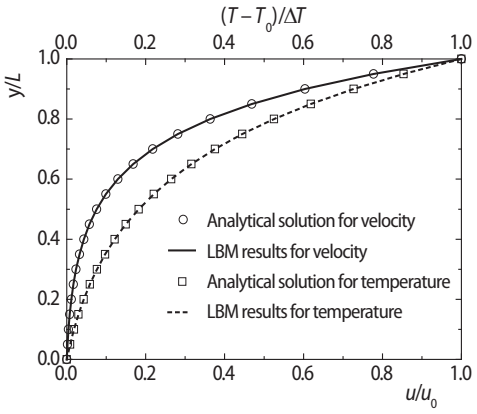

Figure 1. Velocity and temperature profiles in y-direction

$$\frac{u}{u_0} = \frac{e^{Re \cdot y/L} - 1}{e^{Re} - 1} \tag{13}$$

$$\frac{T - T_0}{\Delta T} = \frac{e^{Pr\,Re \cdot y/L} - 1}{e^{Pr \cdot Re} - 1} \tag{14}$$

where u_0 is the velocity of the upper plate, Re – the Reynolds number, ΔT – the temperature difference between the hot and cool plates, Pr – the Prandtl number, and L – the distance between the two plates.

Figure 1 shows the velocity and temperature profiles of numerical simulations and analytical solutions. As shown, the numerical results from the coupled LBM are in highly accordance with the analytical solutions.

Simulation results

Heterogeneity porous media and boundary conditions

The heterogeneity porous media is generated using the QSGS method [11]. The QSGS process is implemented through following steps: the solid seeds distribute randomly in the domain through a seed distribution probability, c_d; each solid seed grows along its eight directions according to each given directional growth probability, D_i; and the growing process of second step is repeated until the desired volume fraction of the growing solid phase. The unoccupied spaces represent the pores at the end.

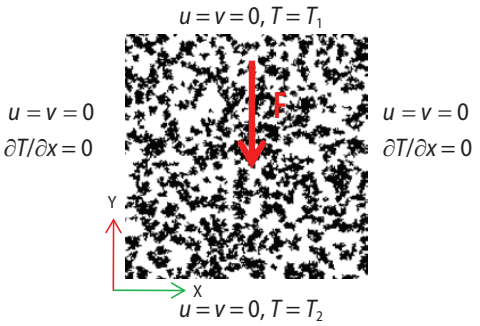

Figure 2. Boundary conditions for heterogeneity porous media; pores (white), impermeable solid (dark), and body-force direction (red arrow) (*for color image see journal web site*)

Figure 2 shows the heterogeneity porous media generated by the QSGS method and boundary conditions for the thermal fluid flow problem. In the complex pore structures, the treatment of fluid-solid interface plays an important role. The half bounce-back boundary condition is employed to obtain the unknown distribution function at the solid-fluid interface with no slip conditions.

Effect of pore structure

Four pore structures with different porosity are studied in this paper and they are shown in fig. 3. The size of four pore structures is 200 × 200 lattices with a resolution of each lattice as 50 nm and their porosity are 0.4, 0.5, 0.6, and 0.7, respectively.

Fluid flow through a heterogeneity porous media is driven by a constant thermal gradient. In the simulations, the Rayleigh number, Prandtl number, and thermal gradient are set as $0.2 \cdot 10^{-5}$, 1.0, and 274 K, respectively. The relaxation parameter and Reynolds number are related to the Reynolds number and Prandtl number. The temperature is set as 0 at the bottom

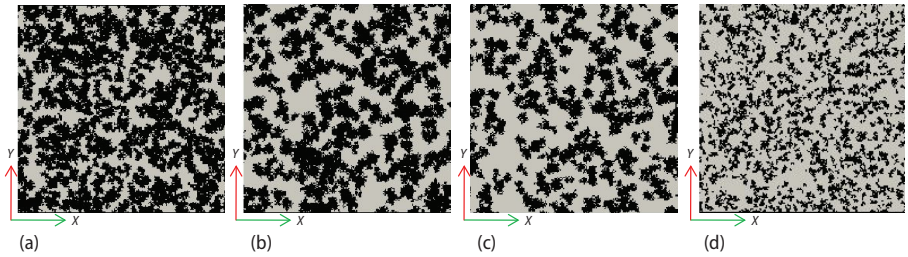

Figure 3. Heterogeneous porous media: (a) 0.4, (b) 0.5, (c) 0.6, and (d) 0.7; pores (gray), impermeable solid (dark)

boundary and the value of the temperature gradient is imposed on the upper boundary. The initial velocity of the fluid is 0 and the average density and the initial density of the fluid are all equal to 1.0, while the lattice speed is 1.0.

The velocity distribution provides the understanding of the fluid flow physics in the confined space. Figure 4 shows the velocity distribution of fluid in four pore structures. As expected, the porosity obviously affects the velocity distribution inside the porous media. For the high porosity structure, the velocity of fluid is widespread inside the porous media, while only a few connected regions have the velocity distribution for the low porosity structure. It

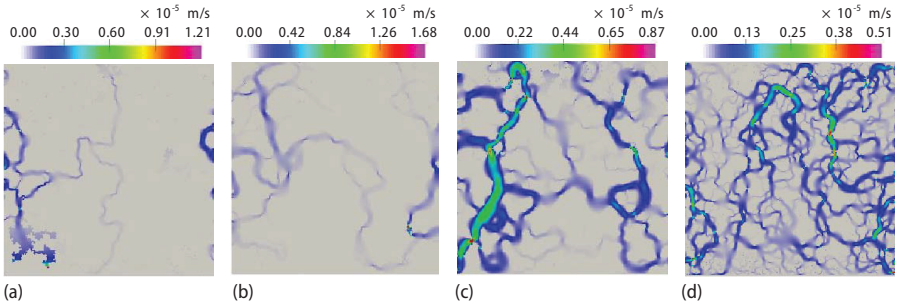

Figure 4. Velocity distribution under different porosity: (a) 0.4, (b) 0.5, (c) 0.6, and (d) 0.7 (*for color image see journal web site*)

can be also found that the maximum velocity decreases with the increasing of porosity. The narrow throats more easily generate in low porosity structure, where fluid molecule and pore wall collisions become more intense resulting in the higher velocity. The flow rate of three cross-sections with different porosity is present in fig. 5. The flow rate increases with the increase of porosity in general, although there are some differences in different cross-sections.

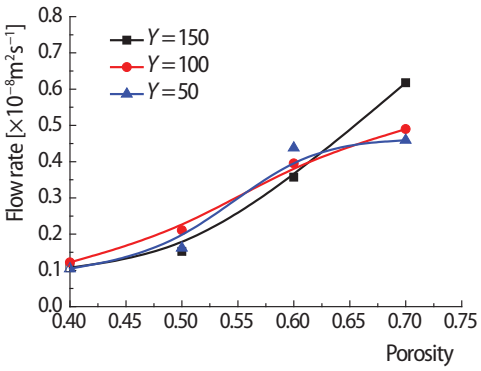

Figure 5. Flow rate under different porosity

Effect of thermal gradient

The effect of the thermal gradient value on fluid flow behavior is simulated in this

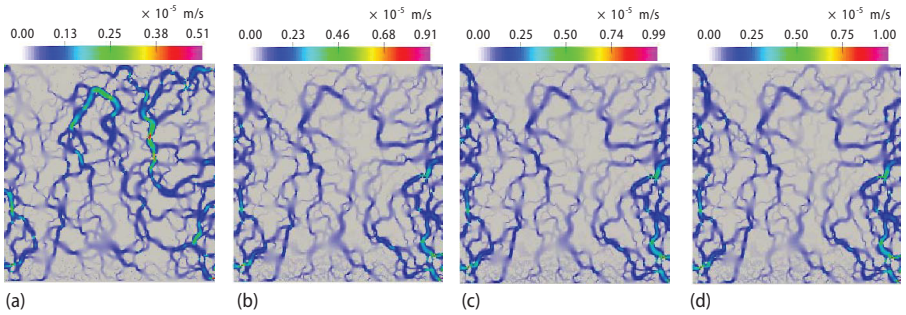

Figure 6. Velocity distribution under different thermal gradient: (a) 274.0 K, (b) 283.0 K, (c) 333.0 K, and (d) 373.0 K
(*for color image see journal web site*)

section. Six thermal gradient values are selected, namely 274.0, 278.0, 283.0, 303.0, 333.0, 373.0 K. The pore structure of porosity 0.7 is chose as the simulated porous media. All other parameters and conditions are kept the same as those used in the previous section.

The velocity distribution under different thermal gradients is shown in fig. 6. The differences of the velocity distribution between thermal gradient 274.0 and 283.0 K can be observed, while the changes in velocity distribution are very small when the thermal gradient is more than 283.0 K. To quantitatively characterize fluid flow behavior, the velocity profile of the fluid at $X = 138$ and flow rate in the cross-sections $Y = 50$ and $Y = 150$ are present in fig. 7. A threshold value of thermal gradient is found in fluid flow induced by thermal effect. Both of the flow velocity and flow rate increase significantly with increasing thermal gradient at the low thermal gradient range and the change in fluid flow is very small when the value of thermal gradient is more than the threshold value.

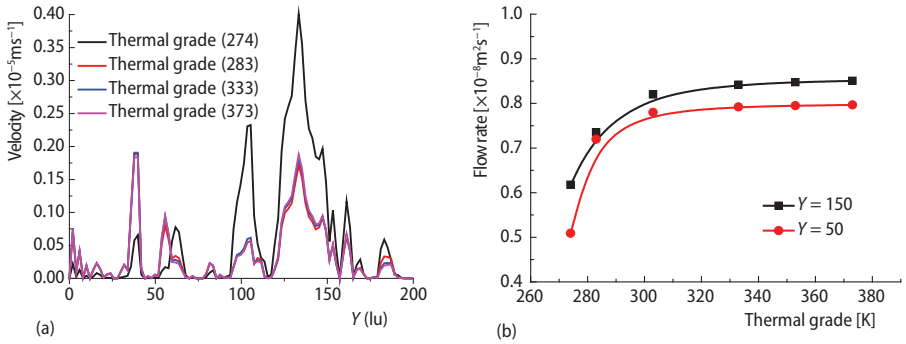

Figure 7. Velocity profiles of the cross section $X = 138$ and flow rate of the cross section $Y = 150$ and $Y = 50$ under different thermal gradient
(*for color image see journal web site*)

Effect of Rayleigh number

Rayleigh number can affect the fluid flow process in heat transfer [10], hence several simulations with different Rayleigh numbers are performed. Four Rayleigh number values are selected, namely $0.2 \cdot 10^5$, $1 \cdot 10^5$, $2 \cdot 10^5$, $5 \cdot 10^5$. Both 274 and 283 K are taken into account. The pore structure of porosity 0.7 is chosen as the simulated porous media. All other parameters and conditions remain unchanged.

Figure 8 shows the velocity distribution at thermal gradient 274 K under different Rayleigh number. Fluid flow induced by thermal effect is strongly related to the Rayleigh number and the maximum flow velocity of fluid clearly increases with the increasing of Rayleigh number, which is consistent with the study result of Guo *et al.* [10]. To quantitatively evaluate the flow velocity in porous media as affected by the Rayleigh number, the velocity profile of the cross-section and flow rate under different Rayleigh number are present in fig. 9. The flow velocity of the cross-section also increases with increasing Rayleigh number. There is a trend towards the increase of the flow rate as the Rayleigh number increases, and the increase is faster at the low Rayleigh number range.

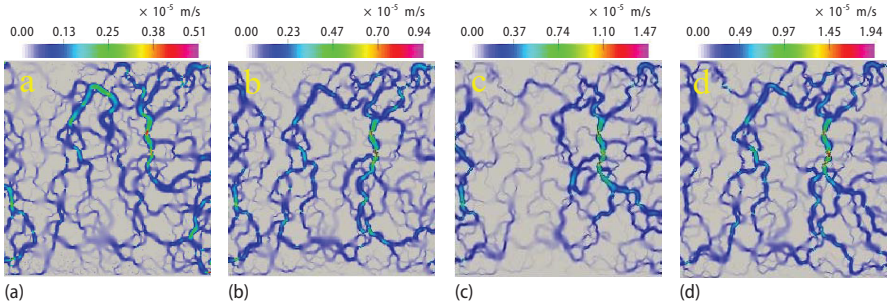

Figure 8. Velocity distribution at thermal grade 274.0 K under different Rayleigh number: (a) $0.2 \cdot 10^5$, (b) $1 \cdot 10^5$, (c) $2 \cdot 10^5$, and (d) $5 \cdot 10^5$
(*for color image see journal web site*)

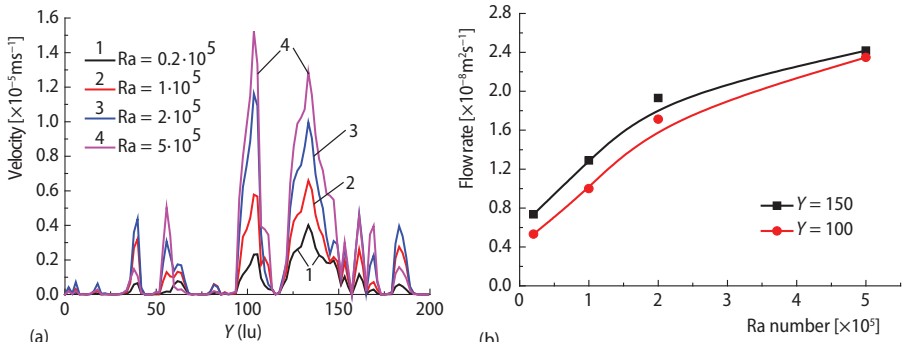

Figure 9. Velocity profiles of the cross-section $X = 138$ at the thermal grade 274.0 K and flow rate of the cross-sections $Y = 150$ and $Y = 100$ at the thermal grade 283.0 K under different Rayleigh number
(*for color image see journal web site*)

Conclusion

In this study, a coupled LBM was adopted to simulate fluid flow induced by thermal effect in heterogeneity porous media. Based on the simulation results, it could be concluded that the geometric properties of heterogeneity porous media play a significant role in controlling the velocity distribution. The low porosity more easily results the high maximum velocity because that the narrow throats more easily generate in low porosity structure, but the flow rate increases with the increase of porosity in general. A threshold of thermal gradient is found in fluid flow induced by thermal effect and the change in fluid flow is very small when thermal gradient is

more than the threshold value. Fluid flow is also strongly related to the Rayleigh number and the increase of the Rayleigh number contributes to improving the flow velocity and flow rate.

Acknowledgment

The authors gratefully acknowledge the financial support of the National Natural Science Foundation of China (No. 51374213, 51674251, 51727807, and 51604263), the National Natural Science Fund for Distinguished Young Scholars of China (No. 51125017), the State Key Research Development Program of China (No. 2016YFC0600705), the Science Fund for Creative Research Groups of the National Natural Science Foundation of China (No. 51421003), the Priority Academic Program Development of the Jiangsu Higher Education Institutions (PAPD 2014), and the Postgraduate Research & Practice Innovation Program of Jiangsu Province (No. KYCX17_1530).

Nomenclature

$\vec{F}$ – body force vector, [N]
Pr – Prandtl number, [–]
Ra – Rayleigh number, [–]
Re – Reynolds number, [–]
T – temperature, [K]
T_0 – reference temperature of fluid, [K]
$\vec{u}$ – fluid velocity vector, [ms^{-1}]

Greek symbols

α_T – thermal expansion coefficient, [K^{-1}]
β – thermal diffusivity, [m^{2}s^{-1}]
ρ – fluid density, [kgm^{-3}]
ρ_0 – reference density of fluid, [kgm^{-3}]
ν – kinematic viscosity, [m^{2}s^{-1}]

References

[1] Shortall, R., *et al.*, Geothermal Energy for Sustainable Development: A Review of Sustainability Impacts and Assessment Frameworks, *Renewable & Sustainable Energy Reviews*, *44* (2015), C, pp. 391-406
[2] Hou, P., *et al*., Experimental Investigation on the Failure and Acoustic Emission Characteristics of Shale, Sandstone and Coal under Gas Fracturing, *Journal of Natural Gas Science and Engineering*, *35* (2016), A, pp. 211-223
[3] Hou, P., *et al*., Changes in Pore Structure and Permeability of Low Permeability Coal under Pulse Gas Fracturing, *Journal of Natural Gas Science and Engineering*, *34* (2016), Aug., pp. 1017-1026
[4] Teng, T., *et al.*, Complex Thermal Coal-Gas Interactions in Heat Injection Enhanced CBM Recovery, *Journal of Natural Gas Science and Engineering*, *34* (2016), Aug., pp. 1174-1190
[5] Yong, Y., *et al*., Numerical Simulation of Gas Diffusion in an Incompressible Thermal Fluid with Lattice Boltzmann Method, (in Chinese), *Journal of Chemical Industry and Engineering, 93* (2012), pp. 93-115.
[6] Liu, H., *et al*., Lattice Boltzmann Simulation of Immiscible Fluid Displacement in Porous Media: Homogeneous *versus* Heterogeneous Pore Network, *Physics of Fluids, 27* (2015), 5, pp. 052103-1-17
[7] Xia, M., Pore-Scale Simulation of Miscible Displacement in Porous Media using the Lattice Boltzmann Method. *Computers & Geosciences, 88* (2016), Mar., pp. 30-40
[8] Chen, S., Doolen, G. D., Lattice Boltzmann Method for Fluid Flows. *Annual Review of Fluid Mechanics, 30* (1998), Jan., pp. 329–364
[9] Guo, Z., Zhao, T., Lattice Boltzmann Model for Incompressible Flows through Porous Media. *Physical Review E, 66* (2002), Sept., 036304
[10] Guo, Z., *et al.*, A Coupled Lattice BGK Model for the Boussinesq Equations. *International Journal for Numerical Method in Fluids, 39* (2002) , 4, pp. 325-342
[11] Wang, M., *et al*., Mesoscopic Predictions of the Effective Thermal Conductivity for Microscale Random Porous Media. *Physical Review E, 75* (2007), Mar., 036702

Paper submitted: March 10, 2017
Paper revised: May 21, 2017
Paper accepted: May 26, 2017